

# Electromagnetic production of $K\Sigma$ on the nucleon near threshold

T. Mart

*Departemen Fisika, FMIPA, Universitas Indonesia, Depok 16424, Indonesia*

(Received 4 August 2014; revised manuscript received 9 November 2014; published 4 December 2014)

Photo- and electroproduction of  $K\Sigma$  have been investigated near their production thresholds by using an effective Lagrangian approach. For this purpose, the background amplitude is constructed from suitable Feynman diagrams, whereas the resonance terms are calculated by means of the Breit–Wigner form of multipoles. Experimental data available in the proton channels ( $K^+\Sigma^0$  and  $K^0\Sigma^+$ ) with energies up to 50 MeV above the thresholds have been utilized to extract the unknown parameters. In these proton channels the calculated observables fit nicely to the experimental data, whereas in the neutron channels ( $K^+\Sigma^-$  and  $K^0\Sigma^0$ ) the predicted observables contain some uncertainties due to the uncertainties in the values of helicity photon couplings. To this end, new  $K^0\Sigma^+$  photoproduction data are urgently required. The present analysis indicates the validity of the  $P_\Lambda = -\frac{1}{3}P_\Sigma$  relation derived a long time ago. In the electroproduction sector the present analysis confirms the smooth transition between photoproduction and low  $Q^2$  electroproduction data. The effect of new Crystal Ball data is shown to be mild at the backward angles. It is also found that the electroproductions of  $K^0\Sigma^+$  and  $K^0\Sigma^0$  are practically not the suitable reactions for investigating the  $K^0$  charge form factor, since the effect is small.

DOI: [10.1103/PhysRevC.90.065202](https://doi.org/10.1103/PhysRevC.90.065202)

PACS number(s): 13.60.Le, 25.20.Lj, 14.20.Gk

## I. INTRODUCTION

Meson photoproduction near its production threshold plays a crucial role in improving our knowledge on the strong interaction involving strangeness degree of freedom, since fewer parameters are involved and, therefore, only fewer uncertainties should be overcome at this kinematics. It is widely known that at energies where the new and precise experimental data points mostly exist there are more than 20 nucleon and 20 delta resonances listed by the Particle Data Group (PDG) [1] in the  $s$  channel of the reaction. There is also a number of hyperon and kaon resonances, in the  $u$  and  $t$  channels, respectively, which should be taken into account for a proper description of the kaon photoproduction process. Unfortunately, almost all of their coupling constants are hardly known and, therefore, must be treated as free parameters fit to experimental data. As the energy increases, the complexity of the problem also increases. For example, at a total center-of-momentum (c.m.) energy  $W$  just above 2 GeV the necessity to include hadronic form factors [2–4] and the phenomenon of Regge behavior seems to be inexorable [5–8]. Clearly, such problems can be efficiently avoided by lowering the considered energy.

In the previous work I analyzed the electromagnetic production of  $K^+\Lambda$  and  $K^0\Lambda$  off a proton for energies up to 50 MeV above the thresholds [9,10]. For this purpose I made use of an effective Lagrangian approach for the background terms and the Breit–Wigner form of multipoles for the resonance terms. Since the excitation energy was limited to 50 MeV above threshold, only the  $N(1650)S_{11}$  state could exist in the resonance terms. However, despite this substantial simplification, there have been very few studies of kaon photoproduction devoted to the threshold region [9–12]. This is understandable, since the corresponding theoretical analysis requires support from accurate experimental data, whereas near the threshold region the cross section tends to be significantly small. Therefore, such a study seemed to be

irrelevant in the past. This situation of course changes with the operation of precise hadron detectors in modern accelerators such as the Continuous Electron Beam Accelerator Facility at the Jefferson Lab (JLab) in Newport News (CEBAF), the 8 GeV Super Photon Ring in Osaka (SPring8), and the Mainz Microtron in Mainz (MAMI).

In this paper I extend my previous analysis [9,10] to the four isospin channels of  $K\Sigma$  photoproduction, i.e., the  $K^+\Sigma^0$ ,  $K^0\Sigma^+$ ,  $K^+\Sigma^-$ , and  $K^0\Sigma^0$  productions. This analysis becomes part of the program for upgrading the phenomenological kaon photo- and electroproduction model, i.e., the Kaon-Maid model [13]. I also believe that it is important to study the processes in details, especially near the production thresholds, where a number of unknown parameters can be easily fixed and many related but important aspects can also be studied. As an example, the electromagnetic form factor of kaon has been shown to produce significant effects near the thresholds of the  $K^+\Lambda$  and  $K^0\Lambda$  channel [9,10]. Considering fewer uncertainties at this kinematics, my previous analyses obviously encourage investigation of the kaon charge form factors at thresholds. Furthermore, by using the method developed in Refs. [14,15], the small structure appearing at  $W \approx 1.65$  GeV in the  $K^+\Lambda$  polarization observable provides important evidence of a new missing resonance or a narrow resonance [16] predicted by the chiral quark soliton model [17].

The four isospin channels of  $K\Sigma$  photoproduction along with their threshold energies are given in Table I. It is apparent that photoproduction of  $K\Sigma$  is similar to the photoproduction of pion-nucleon ( $\pi N$ ), because it involves the production of isospin 1 and isospin  $\frac{1}{2}$  hadrons. However, the difference is also obvious, i.e., in the case of kaon (pion) the  $\Sigma$  hyperon ( $\pi$  meson) has isospin 1, whereas the  $K$  meson (nucleon) has isospin  $\frac{1}{2}$ . Besides that, the presence of explicit strangeness in the case of kaon makes kaon photoproduction more unique than pion photoproduction.

There have been extensive discussions in the literature [8,18–29] about strangeness photoproduction which provides

TABLE I. Threshold energies of the  $K\Sigma$  photoproductions off the proton in terms of the photon laboratory energy ( $E_\gamma^{\text{thr.}}$ ) and the total c.m. energy ( $W^{\text{thr.}}$ ).

No.	Channel	$E_\gamma^{\text{thr.}}$ (MeV)	$W^{\text{thr.}}$ (MeV)
1	$\gamma + p \longrightarrow K^+ + \Sigma^0$	1046	1686
2	$\gamma + p \longrightarrow K^0 + \Sigma^+$	1048	1687
3	$\gamma + n \longrightarrow K^+ + \Sigma^-$	1052	1691
4	$\gamma + n \longrightarrow K^0 + \Sigma^0$	1051	1690

a new mechanism to investigate the so-called missing resonances, i.e., the resonances predicted by quark models but not listed by the PDG [1], since it does not appear in the pion-nucleon scattering process. This is due to the fact that their decay widths are only sizable to the strangeness channels, rather than to the  $\pi N$  channels [30]. An example of such efforts has been performed for the  $K^+\Lambda$  channel, where a  $D_{13}(1895)$  as a candidate of the missing nucleon resonance [27] was concluded from an analysis of the second peak in the cross section of the  $K^+\Lambda$  photoproduction data from the SAPHIR 1998 [31]. Note that different conclusions, however, could be drawn by using recent experimental data [20]. Recently, it was found that the peak originates mostly from the contribution of  $P_{13}(1900)$ , instead of the  $D_{13}(1895)$  [24,32].

Furthermore, there is an intrinsic difference between photoproductions of  $K\Sigma$  and  $K\Lambda$ , which comes from the consequence of the hyperon isospin in the final states. Since  $\Sigma$  is an isovector particle, photoproduction of  $K\Sigma$  yields a total isospin  $\frac{3}{2}$  in the final state and, as a consequence, allows for isospin  $\frac{3}{2}$  ( $\Delta$ ) intermediate states in the  $s$  channel. Thus, photoproduction of  $K\Sigma$  would provide more information not available from photoproduction of  $K\Lambda$ . Although the number of resonances increases with the inclusion of  $\Delta$  resonances, the total number of resonances used in the present investigation is only four, in which only one  $\Delta$  resonance is relevant, i.e.,  $\Delta(1700)D_{33}$ .

Photoproduction of  $K\Sigma$  was first considered more than 50 years ago in the lowest-order perturbation theory by exploiting very modest information on the spin, parity, and coupling constants of both kaon and hyperon [33]. By normalizing the leading coupling constants ( $g_{K\Lambda N}/\sqrt{4\pi}$  and  $g_{K\Sigma N}/\sqrt{4\pi}$ ) to unity a number of cross sections for different photon energies were calculated. At the same time, a similar calculation was also made with variation of coupling constants [34]. However, investigation of  $K\Sigma$  channels began to be more attractive only after the finding of Ref. [35], which showed that the available phenomenological models for the  $K^+\Sigma^0$  process overpredict the  $K^0\Sigma^+$  cross section by almost two orders of magnitude. Only after including very few  $K^0\Sigma^+$  data in the fit, this problem can be partly alleviated. Unfortunately, the extracted leading coupling constants are too small and cannot be reconciled with the prediction of SU(3) and those extracted from the kaon scattering processes [35]. Since most of the contributions come from the Born terms, introducing hadronic form factors in hadronic vertices of the scattering amplitude might become the suitable choice. There is a number of recipes proposed in the literature for including these form factors

without destroying the gauge invariance of the process [2]. In spite of significant improvements in the model, the inclusion of hadronic form factors simultaneously oversuppresses the cross section at very forward angles [36]. Furthermore, different methods to suppress the excessively large Born terms also exist in the literature. For instance, Ref. [37] proposed the use of hyperon resonances, instead of hadronic form factors, to overcome the large contribution of background terms. Meanwhile, within the framework of the chiral quark model (CQM), Ref. [38] showed that the inclusion of higher-mass and -spin resonances could also overcome the problem of the  $K^0\Sigma^+$  cross section overprediction, since the  $\Delta(1905)F_{35}$ ,  $\Delta(1910)P_{31}$ ,  $\Delta(1920)P_{33}$ , and  $\Delta(1950)F_{37}$  resonances have been shown to yield a minimum at  $W \approx 1.9$  GeV [38].

In contrast to the  $K^+\Lambda$  channel, where the problem of data consistency has severely plagued phenomenological analyses for years [39,40], experimental data of the  $K^+\Sigma^0$  channel from SAPHIR 2004 [41], CLAS 2006 [42], and CLAS 2010 [43] seem to be consistent. Thus, the number of available experimental data near threshold in this channel is relatively large, improving the accuracy of the present analysis.

The organization of this paper is as follows: In Sec. II, I briefly present the formalism used in my analysis. In Sec. III, I discuss the numerical result obtained for the  $K\Sigma$  photoproduction. Section IV presents the effect of the new Crystal Ball data on my calculation. The result for the electroproduction case is given in Sec. V. Section VI is exclusively devoted to discussing the recent MAMI electroproduction data at very low  $Q^2$ . In Sec. VII, I briefly discuss the effect of the  $K^0$  charge form factor on the cross sections of the  $K^0\Sigma^+$  and  $K^0\Sigma^0$  channels. I summarize my present analysis and conclude my finding in Sec. VIII. A small portion of the results obtained in the present analysis, which uses the older PDG information [44], has been presented in conferences [45,46]. The present paper reports on the comprehensive result of this analysis. Furthermore, here I use the information of nucleon resonances obtained from the latest PDG data [1], which leads to a slightly different result in the extracted nucleon-resonance properties as well as in the calculated observables.

## II. FORMALISM

A complete formalism of the background and resonance amplitudes for the  $\gamma + p \rightarrow K^+ + \Lambda$  channel has been written in my previous paper [9]. For use in the four channels  $K\Sigma$  photoproduction, a number of modifications is needed. This includes the the isospin relation of hadronic coupling constants in the background terms [35], i.e.,

$$g_{K^+\Sigma^0 p} = -g_{K^0\Sigma^0 n} = g_{K^0\Sigma^+ p}/\sqrt{2} = g_{K^+\Sigma^- n}/\sqrt{2}, \quad (1)$$

$$g_{K^+\Lambda p} = g_{K^0\Lambda n}, \quad g_{K^{*+}\Lambda p} = g_{K^{*0}\Lambda n}, \quad (2)$$

as well as the isospin factor

$$c_{K\Sigma} = \begin{cases} -1/\sqrt{3}, & \text{isospin } \frac{1}{2} \\ \sqrt{3}/2, & \text{isospin } \frac{3}{2} \end{cases} \quad (3)$$

of the multipoles [47] in the resonance terms, i.e.,

$$A_{\ell\pm}^R(W) = \bar{A}_{\ell\pm}^R c_{K\Sigma} \frac{f_{\gamma R}(W) \Gamma_{\text{tot}}(W) M_R f_{KR}(W)}{M_R^2 - W^2 - iM_R \Gamma_{\text{tot}}(W)} e^{i\phi}, \quad (4)$$

where the total width  $\Gamma_{\text{tot}}$  can be related to the resonance width ( $\Gamma_R$ ) by using Eq. (11) of Ref. [39]. Further explanation of Eq. (4) can be found in Sec. II of Ref. [39].

In the case of resonance contribution I adopt the convention of pion photo- and electroproduction [47] for the physical amplitudes of the kaon photo- and electroproduction, i.e.,

$$A(\gamma + p \rightarrow K^+ + \Sigma^0) = A_p^{(1/2)} + \frac{2}{3}A^{(3/2)}, \quad (5)$$

$$A(\gamma + p \rightarrow K^0 + \Sigma^+) = \sqrt{2} \left[ A_p^{(1/2)} - \frac{1}{3}A^{(3/2)} \right], \quad (6)$$

$$A(\gamma + n \rightarrow K^+ + \Sigma^-) = \sqrt{2} \left[ A_n^{(1/2)} + \frac{1}{3}A^{(3/2)} \right], \quad (7)$$

$$A(\gamma + n \rightarrow K^0 + \Sigma^0) = -A_n^{(1/2)} + \frac{2}{3}A^{(3/2)}, \quad (8)$$

where  $A_p^{(1/2)}$  and  $A_n^{(1/2)}$  are the proton and neutron amplitudes with total isospin  $\frac{1}{2}$ , respectively, whereas  $A^{(3/2)}$  is the amplitude for the isospin  $\frac{3}{2}$  contribution. The formalism given by Eqs. (5)–(8) can be implemented in the calculation of the Chew—Goldberger—Low—Nambu (CGLN) amplitudes  $F_1, \dots, F_6$  [47] from the multipoles before calculating the cross section or polarization observables. Note that, by limiting the energy up to 50 MeV above the production thresholds, the number of electric, magnetic, and scalar multipoles is significantly limited. As a consequence, the relation between CGLN amplitudes and the multipoles can be simplified to

$$F_1 = E_{2-} + 3M_{2-} + 3(E_{1+} + M_{1+}) \cos \theta, \quad (9)$$

$$F_2 = 2M_{1+} + M_{1-} + 6M_{2-} \cos \theta, \quad (10)$$

$$F_3 = 3(E_{1+} - M_{1+}), \quad (11)$$

$$F_4 = -3(M_{2-} + E_{2-}), \quad (12)$$

$$F_5 = S_{1-} - 2S_{1+} + 6S_{2-} \cos \theta, \quad (13)$$

$$F_6 = 6S_{1+} \cos \theta - 2S_{2-}. \quad (14)$$

Since both proton and neutron channels exist in  $K\Sigma$  photoproduction, I obviously need the ratios between charged and neutral kaon transition moments  $r_{K^*K\gamma} \equiv g_{K^*K^0\gamma}/g_{K^*K^+\gamma}$  and  $r_{K_1K\gamma} \equiv g_{K_1^0K^0\gamma}/g_{K_1^+K^+\gamma}$ . The first ratio can be fixed by using the PDG values [1], whereas the second ratio can be considered as a free parameter during the fit process because, fortunately, one of the proton channels that produces neutral kaon ( $\gamma + p \rightarrow K^0 + \Sigma^+$ ) has experimental data, although very limited. A more detailed discussion about this topic will be given when I discuss the result of the  $K^0\Sigma^+$  channel in Sec. III.

Note that the electromagnetic vertices of hyperon resonances in the charged hyperon productions ( $K^0\Sigma^+$  and  $K^+\Sigma^-$ ) are different from those in the neutral hyperon productions ( $K^+\Sigma^0$  and  $K^0\Sigma^0$ ). Figure 1 exhibits the corresponding coupling constants for all  $\Sigma$  channels. The hadronic part of the coupling constants,  $g_{K^*N}$ , are obviously related by using Eq. (1), whereas the electromagnetic coupling  $g_{Y^*\gamma\Sigma}$  depends on the charge of the hyperon. Obviously, the neutral hyperon ( $\Sigma^0$ ) productions use the same  $g_{Y^*0\gamma\Sigma^0}$  coupling, while the charged hyperon ( $\Sigma^+, \Sigma^-$ ) productions use the same  $g_{Y^{*\pm}\gamma\Sigma^\pm}$

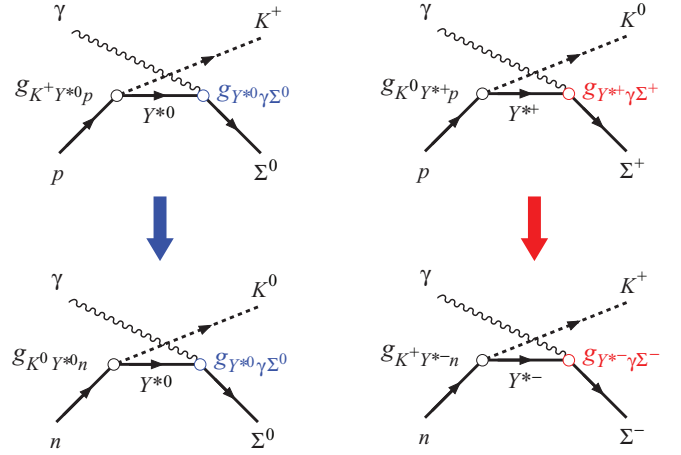


FIG. 1. (Color online) Hadronic and electromagnetic coupling constants in the hyperon resonance intermediate state of  $K\Sigma$  photoproductions. Whereas the hadronic coupling constants are related through Eq. (1), the electromagnetic coupling constants of the charged  $\Sigma$  production is different from that of the neutral  $\Sigma$  production.

coupling. Thus, in the fitting process one can use the ratio  $c_{Y^*} \equiv g_{Y^{*\pm}\gamma\Sigma^\pm}/g_{Y^*0\gamma\Sigma^0}$  as a free parameter to distinguish the charged hyperon resonance from the neutral one.

Note that the above formalism is also valid in the case of electroproduction. To this end I use the standard electromagnetic form factors as in my previous work [9,10] for the extension of my model to the finite- $Q^2$  region, where  $Q^2$  is the square of the virtual photon momentum. As in the previous work [9] I do not use the hadronic form factor in the present work because the energy considered is sufficiently low and, as a consequence, agreement between model calculation and experimental data can be easily achieved.

As in the previous study I consider the energies from the production threshold ( $W \simeq 1690$  MeV) up to 50 MeV above the threshold ( $W \simeq 1740$  MeV). In this energy range there are three nucleon and one  $\Delta$  resonances in the PDG listing, i.e., the  $N(1700)D_{13}$ ,  $\Delta(1700)D_{33}$ ,  $N(1710)P_{11}$ , and  $N(1720)P_{13}$  resonances. Their properties relevant to the present study are listed in Table II. Properties of the particles as well as other parameters used in the background terms can be found in my previous work [9]. Due to the nature of resonance formalism used in the present study [47], the nucleon resonances with masses below the threshold energies cannot be included as in the case of the covariant formalism [48].

There are 331 experimental data points in the database, dominated by the  $K^+\Sigma^0$  photoproduction differential cross section [41–43,49]. In addition, there are also data for the  $K^+\Sigma^0$  electroproduction differential cross section [50],  $K^0\Sigma^+$  photoproduction differential cross section [51], and  $K^+\Sigma^0$  recoil polarization [41,43]. Other data, such as from the  $K^+\Sigma^0$  and  $K^+\Sigma^-$  photoproduction measurement by the LEPS collaboration [52,53], have photon energies beyond the upper limit of the present analysis. Note that the number of data points in the  $K\Sigma$  production near threshold is larger than that

TABLE II. Properties of the nucleon resonances used in the present analysis [1].  $M_R$  and  $\Gamma_R$  are the mass and width of the resonance, respectively,  $A_{1/2}$  and  $A_{3/2}$  are the resonance photodecay helicity amplitudes, and  $\beta_{K\Lambda}$  is the kaon branching ratio to the  $K\Lambda$  channel. See Sec. III of Ref. [9] for further explanation of these Breit–Wigner resonance parameters. The status of the resonance is given by a number of asterisks (\*) according to the PDG. Further explanation of this status can be found in Ref. [1].

Resonance	$N(1700)D_{13}$	$\Delta(1700)D_{33}$	$N(1710)P_{11}$	$N(1720)P_{13}$
$M_R$ (MeV)	$1700 \pm 50$	$1700^{+50}_{-30}$	$1710 \pm 30$	$1720^{+30}_{-20}$
$\Gamma_R$ (MeV)	$150^{+100}_{-50}$	$300 \pm 100$	$100^{+150}_{-50}$	$250^{+150}_{-100}$
$\beta_{K\Lambda}$	$<0.03$		$0.15 \pm 0.10$	$0.044 \pm 0.004$
$A_{1/2}(p)$ ( $10^{-3}$ GeV $^{-1/2}$ )	$+15 \pm 25$	$+140 \pm 30$	$+40 \pm 20$	$+100 \pm 20$
$A_{3/2}(p)$ ( $10^{-3}$ GeV $^{-1/2}$ )	$-15 \pm 25$	$+140 \pm 30$		$+150 \pm 30$
$A_{1/2}(n)$ ( $10^{-3}$ GeV $^{-1/2}$ )	$+20 \pm 15$	$+140 \pm 30$	$-40 \pm 20$	$+7 \pm 15$
$A_{3/2}(n)$ ( $10^{-3}$ GeV $^{-1/2}$ )	$-30 \pm 20$	$+140 \pm 30$		$-5 \pm 25$
Overall status	***	****	***	****
Status seen in $K\Sigma$	*	*	*	*

in the  $K\Lambda$  case [9] (139 data points). Thus, the better statistics obtained from the present analysis could be expected.

### III. RESULT FOR PHOTOPRODUCTION

The parameters extracted from the fit to 331 data points are displayed in Tables III and IV, where the background and resonance parameters are separated in different tables for the sake of convenience. Note that the effect of the  $\Lambda(1800)S_{01}$  resonance, which was found to play important role in the  $K^+\Lambda$  photoproduction near threshold [9] as well as at higher photon energies [54], have also been investigated. In the present work it is found that the effect is almost negligible, i.e.,  $\chi^2/N$  is reduced from 1.07 to 1.05, whereas other extracted parameters do not dramatically change after including the  $\Lambda(1800)S_{01}$  resonance (see Table III). Therefore, in the following discussion the hyperon resonance will be excluded.

TABLE III. Extracted background parameters from fit to experimental data by excluding and including the  $\Lambda(1800)S_{01}$  hyperon resonance (indicated by  $Y^*$ ). Note that, during the fits, the main coupling constants  $g_{K\Lambda N}/\sqrt{4\pi}$  and  $g_{K\Sigma N}/\sqrt{4\pi}$  were varied within the values accepted by the SU(3) prediction with a 20% symmetry breaking [55].

Coupling constants	Without $Y^*$	With $Y^*$
$g_{K\Lambda N}/\sqrt{4\pi}$	-3.18	-3.00
$g_{K\Sigma N}/\sqrt{4\pi}$	1.30	1.30
$G_{K^*}^V/(4\pi)$	-0.02	-0.04
$G_{K^*}^T/(4\pi)$	-0.32	-0.32
$G_{K_1}^V/(4\pi)$	-0.03	-0.14
$G_{K_1}^T/(4\pi)$	-0.04	-0.32
$G_{Y^*}/(4\pi)$		-1.70
$r_{K_1 K\gamma}$	2.99	2.07
$c_{Y^*}$		1.33
$\Lambda_K$ (GeV)	1.63	1.63
$\Lambda_{K^*}$ (GeV)	0.50	0.50
$\Lambda_{K_1}$ (GeV)	0.50	0.50
$\Lambda_Y$ (GeV)	0.50	0.50
$\chi^2/N$	1.07	1.05

Table III indicates that contributions of the  $K^*(892)$  and  $K_1(1270)$  vector mesons are relatively small, which is in contrast to the case of  $K\Lambda$  production [9]. The extracted ratio  $r_{K_1 K\gamma} = 2.99$  is obviously larger than that obtained in Kaon-Maid, i.e.,  $-0.45$ . The extracted  $r_{K_1 K\gamma}$  decreases when the  $\Lambda(1800)S_{01}$  hyperon resonance is included in the model (see Table III). This issue will be discussed later in this section.

The achieved  $\chi^2$  per degree of freedom is close to one, indicating that the omission of hadronic form factors in the present analysis does not lead to a serious problem, as in the analyses beyond the threshold region. The extracted resonance properties shown in Table IV do not show any dramatic deviations from the PDG values since, during the fit, they were varied within the error bars given by the PDG [1].

Comparison between contributions of the background and resonance terms is displayed in Fig. 2. It is obvious from this figure that contribution of the background terms is dominant in the  $K^+\Sigma^0$  and  $K^0\Sigma^0$  channels, which can be understood as the isospin effects in the background amplitudes given by Eqs. (1) and (2). In contrast to this, the effect of resonances clearly shows up in both the  $K^0\Sigma^+$  and  $K^+\Sigma^-$  channels. This phenomenon is also understood from the isospin factors in the resonances given by Eqs. (6) and (7).

A comparison between the predicted total cross sections and those from previous works [11,13] as well as experimental data [41,42,51] is shown in Fig. 3. It is obvious that the present analysis provides a more accurate prediction in both proton channels ( $K^+\Sigma^0$  and  $K^0\Sigma^+$ ). In the neutron channels ( $K^+\Sigma^-$  and  $K^0\Sigma^0$ ) the cross-section uncertainties are found to be relatively large, as shown by the shaded area in the right panels of Fig. 3, especially at  $W \approx 1700$  MeV, where most of the involved resonances are located. Note that all uncertainties shown in the right panels of Fig. 3 originate from the uncertainties in the neutron helicity amplitudes  $A_{1/2}(n)$  and  $A_{3/2}(n)$  given by the PDG (see Table II) [1]. Thus, experimental data in both neutron channels are urgently required to reduce this uncertainty. Such experimental data could be expected from the  $K^0$  photoproduction experiment performed by the Tohoku group which uses deuteron as a target [56]. Nevertheless, for this purpose, higher-statistics data are more recommended in order to reduce some uncertainties coming from the Fermi motion in the deuteron as well as from the final-state interaction

TABLE IV. Extracted resonance parameters from fit to experimental data.  $\beta_{K\Sigma}$  is the kaon branching ratio to the  $K\Sigma$  channel,  $\phi$  is the Breit-Wigner resonance parameter given in Eq. (7) of Ref. [9], whereas  $\alpha_{N^*}$  and  $\beta_{N^*}$  are the parameters of the  $Q^2$  dependence of the resonance multipoles given by Eq. (18) in Sec. V.

Resonance	$N(1700)D_{13}$	$\Delta(1700)D_{33}$	$N(1710)P_{11}$	$N(1720)P_{13}$
$M_R$ (MeV)	1716	1692	1727	1700
$\Gamma_R$ (MeV)	250	400	50	150
$\beta_{K\Sigma}$	$3.0 \times 10^{-2}$	$6.4 \times 10^{-5}$	$5.5 \times 10^{-3}$	$1.2 \times 10^{-4}$
$\phi$ (deg)	163	63	40	360
$A_{1/2}(p)$ ( $10^{-3}$ GeV $^{-1/2}$ )	40	170	43	120
$A_{3/2}(p)$ ( $10^{-3}$ GeV $^{-1/2}$ )	-6	110		120
$S_{1/2}(p)$ ( $10^{-3}$ GeV $^{-1/2}$ )	-27	-100	26	-100
$\alpha_{N^*}$ (GeV $^{-2}$ )	0.00	3.86	2.98	9.93
$\beta_{N^*}$ (GeV $^{-2}$ )	1.44	3.07	1.98	2.77

induced by the spectator nucleon. For the  $K^+\Sigma^-$  photoproduction off a deuteron, experimental data have been available from the CLAS collaboration with photon lab energies from 1.1 GeV (almost 50 MeV above the threshold; see Table I) up to 3.6 GeV [57]. Although the lowest energy is very close to the upper limit of the present analysis, the challenging task now is to remove the effects of initial- and final-state interactions from the data.

A comparison between the calculated differential cross section of the  $K^+\Sigma^0$  channel with the prediction of Kaon-Maid [13] and experimental data [41–43] is shown in Fig. 4. Within the existing experimental error bars the present work also provides a significant improvement to the result of Kaon-Maid, especially at  $W = 1735$  and  $1745$  MeV. Further improvement can also be observed in the forward directions. Note that, in Kaon-Maid, the problem in this kinematics originates from the inclusion of hadronic form factors, which oversuppress the  $K\Lambda$  cross sections at forward angles [36]. Therefore,

the present study also emphasizes the need for a thorough investigation of the effects of including hadronic form factors on differential cross sections at forward kinematics.

Differential cross sections of the  $\gamma + p \rightarrow K^0 + \Sigma^+$  process display an interesting result. Unlike the prediction of Kaon-Maid, which is almost similar to the  $K^+\Lambda$  case, here the cross sections rise sharply in the backward directions and reach the minima at  $\theta_K \simeq 90^\circ$ . The cross section enhancement is also detected at forward angles. The result indicates a strong

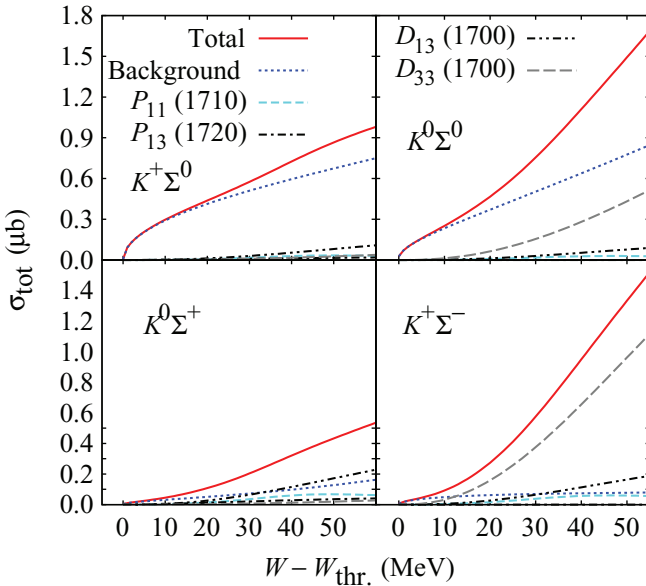


FIG. 2. (Color online) Contribution of the background,  $N(1710)P_{11}$ ,  $N(1720)P_{13}$ ,  $N(1700)D_{13}$ , and  $\Delta(1700)D_{33}$  resonance amplitudes to the total cross section of the  $\gamma + N \rightarrow K\Sigma$  processes in four isospin channels.

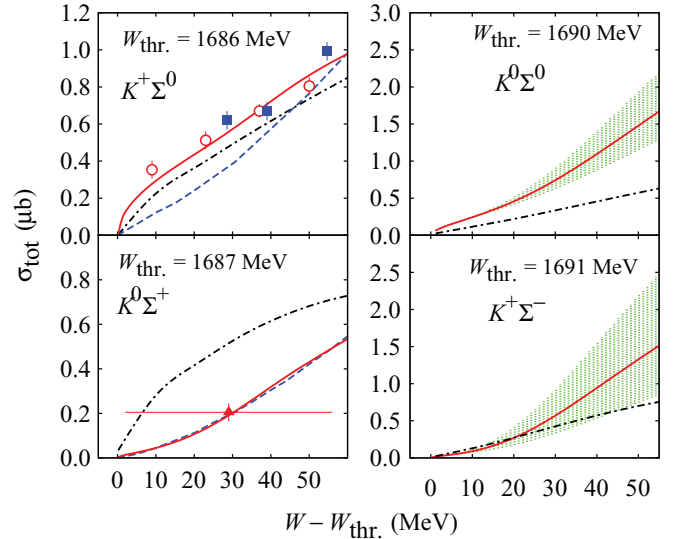


FIG. 3. (Color online) Total cross section obtained in the present work (solid lines) compared with the results of Kaon-Maid [13] (dashed-dotted lines) and chiral perturbation theory (CHPT) [11] (dashed lines) as well as the available experimental data from the SAPHIR collaboration (open circles [41] and solid triangle [51]), and the CLAS collaboration (solid squares [42]). In the case of the  $K^0\Sigma^0$  and  $K^+\Sigma^-$  channels (right panels), the uncertainties of the present calculations, due to the uncertainties in the helicity photon couplings of the resonances given in Table II, are indicated by the shaded green areas. If these uncertainties are excluded, the result is shown by the solid lines. Note that both the present work and Kaon-Maid do not include the total-cross-section data shown in this figure in the fitting database. The CHPT uses the leading coupling constants predicted by SU(3) as the input for calculating this cross section.

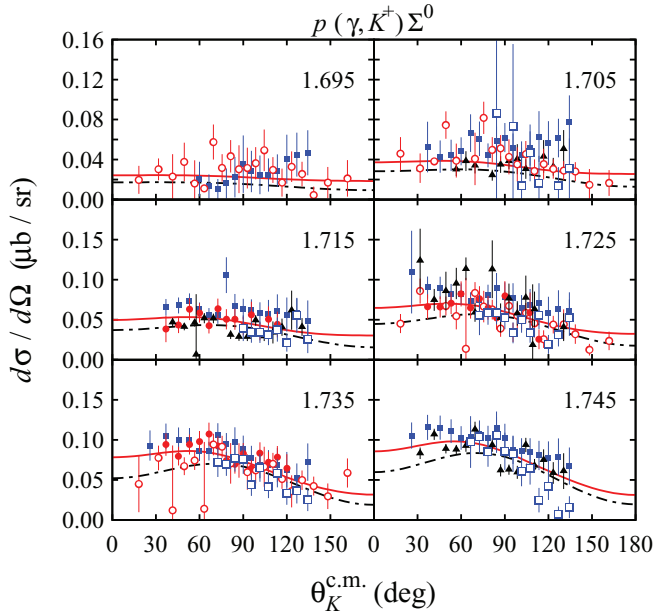


FIG. 4. (Color online) Comparison between angular distributions of the  $\gamma + p \rightarrow K^+ + \Sigma^0$  differential cross section obtained from the present and Kaon-Maid [13] models with experimental data from the SAPHIR (open circles [41]), CLAS (solid squares [43], solid circles [42], and solid triangles [49]), and Crystal Ball (open squares [58]) collaborations. The corresponding total c.m. energy  $W$  (in GeV) is shown in each panel. Except for the new Crystal Ball data, all experimental data displayed in this figure were used in the fit to obtain the solid line.

$u$ -channel contribution which is solely mediated by the  $\Sigma^+$  (since the  $\Sigma^*$  resonances do not significantly contribute and therefore are not included in the model) as well as important contributions from the  $t$ -channel intermediate states obtained from the  $K^{0*}$  and  $K_1^0$  meson resonances.

Photoproduction of  $K^0\Sigma^+$  is especially important for the extraction of the ratio between the  $K_1(1270)$  transition moments in  $K^0$  and  $K^+$  productions, i.e.,

$$r_{K_1K\gamma} \equiv g_{K_1^0K^0\gamma}/g_{K_1^+K^+\gamma}, \quad (15)$$

since there is no information available for the  $K_1 \rightarrow K\gamma$  decay width. This is in contrast with the lower-mass vector meson, the  $K^*(892)$ , since the PDG provides the values of both the  $K^{*+} \rightarrow K^+\gamma$  and  $K^{0*} \rightarrow K^0\gamma$  decay widths [1], which can be related to their transition strengths by means of [59]

$$\Gamma_{K^* \rightarrow K\gamma} = \frac{9.8 \text{ MeV}}{4\pi} |g_{K^*K\gamma}|^2, \quad (16)$$

whereas its sign can be constrained by using the cloudy bag model computation by Singer and Miller [60].

In the present work, the value of  $r_{K_1K\gamma}$  is found to be 2.99 (see Table III). In Kaon-Maid this value was obtained to be  $-0.45$  [10]. The presently extracted  $r_{K_1K\gamma}$  is larger presumably because the contribution of  $K_1(1270)$  would be different for different models. The discrepancy between the two values could originate from the small number of  $K^0\Sigma^+$  data used in the database. In the present work the available data for the  $\gamma + p \rightarrow K^0 + \Sigma^+$  channel near threshold are merely 10

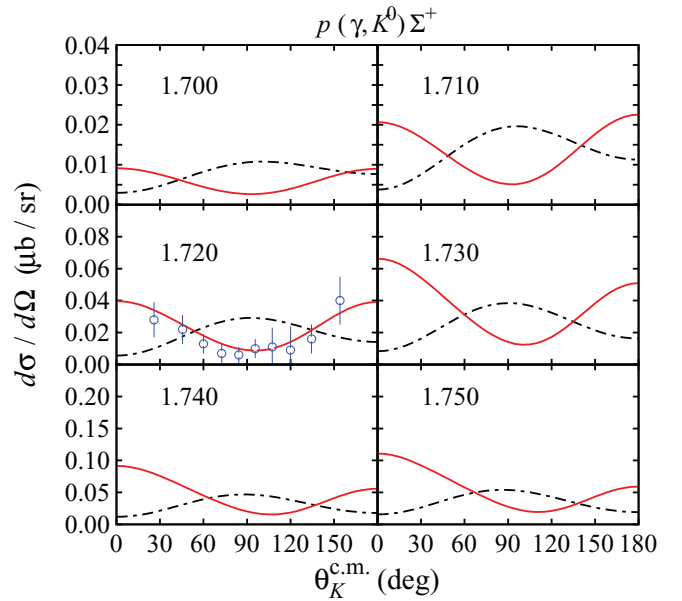


FIG. 5. (Color online) Angular distribution of the  $\gamma + p \rightarrow K^0 + \Sigma^+$  differential cross sections. Notation of the curves is as in Fig. 4. Experimental data at  $W = 1720$  MeV are from the SAPHIR Collaboration [51].

points as shown in Fig. 5, whereas Kaon-Maid used only 29 data points in its database. As shown in Ref. [10], this ratio is required for extending the  $K^+\Lambda$  photoproduction model to include the  $K^0\Lambda$  channel. In the pseudoscalar theory it was found that variation of this ratio changes the cross section only at higher energies. However, the effect is substantially large in the case of pseudovector coupling. It is also apparent that, by including the new Crystal Ball data (to be discussed in Sec. IV), a smaller ratio, i.e.,  $r_{K_1K\gamma} = 2.07$ , would be obtained, which is in principle approaching the value of Kaon-Maid. This happens because the new Crystal Ball data are closer to the SAPHIR data, instead of the CLAS data (see Sec. IV), whereas Kaon-Maid was fit to the the SAPHIR data [31].

In order to investigate the sensitivity of the calculated cross sections depicted in Fig. 5 to the  $r_{K_1K\gamma}$  ratio, the calculated cross sections are replotted in Fig. 6. Figure 6 shows the cross-section changes if the ratio is varied within  $\pm 20\%$ . Obviously, sizable variations can be observed at the forward and backward angles. Nevertheless, the presently available data cannot resolve this variation. Therefore, it is urgent to measure this channel in order to improve our understanding on the  $K\Sigma$  photoproduction. With about 10% error bars the experimental data would be able to constrain this ratio to vary within less than 20% of its value. Meanwhile, a photoproduction experiment has been performed off a proton target by the CLAS collaboration at JLab. Data with very high statistics have been collected and will be analyzed in the near future [61]. Precise data on the  $\gamma + p \rightarrow K^0 + \Sigma^+$  channel would allow us to extract not only the  $r_{K_1K\gamma}$  ratio, but also the corresponding ratio for the  $K^*(892)$  vector meson. Therefore, a more stringent constraint could also be imposed on both the  $K^{*+} \rightarrow K^+\gamma$  and  $K^{0*} \rightarrow K^0\gamma$  decay widths.

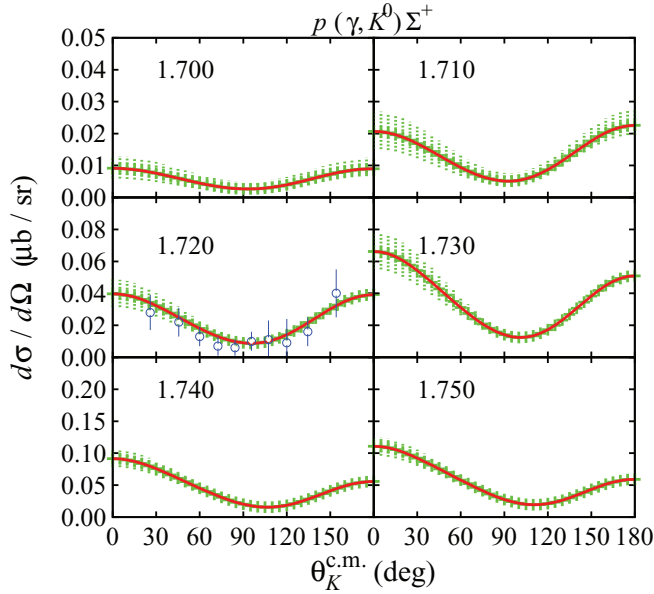


FIG. 6. (Color online) Variation in the differential cross section of the  $\gamma + p \rightarrow K^0 + \Sigma^+$  process as a result of 20% variation of the  $r_{K^1 K \gamma}$  values. Note that the variation is indicated by the green shaded area. Solid lines indicate the cross section calculated without this variation. Experimental data are the same as in Fig. 5.

Figures 7 and 8 display the predicted differential cross section of the  $K^+\Sigma^-$  and  $K^0\Sigma^0$  channels, respectively, where the prediction of Kaon-Maid is also shown for comparison. In the  $K^+\Sigma^-$  channel, except for the lowest energy, the predictions of both Kaon-Maid and the present work are in agreement with each other, whereas in the case of the  $K^0\Sigma^0$

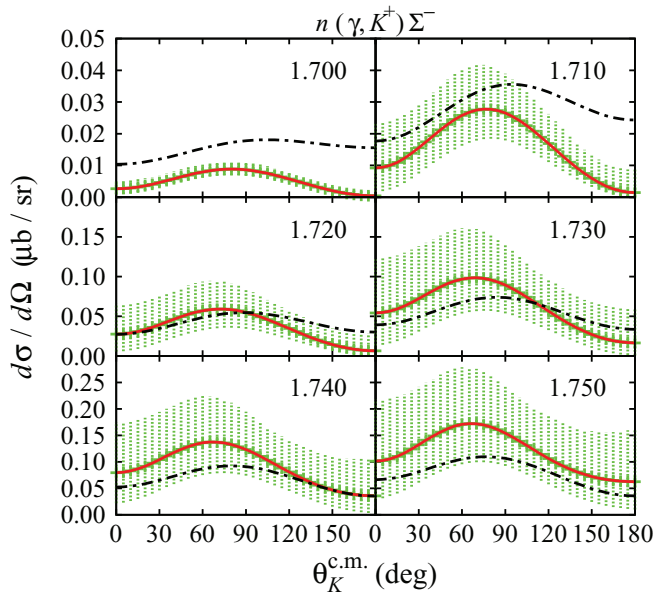


FIG. 7. (Color online) As in Fig. 5 but for the  $\gamma + n \rightarrow K^+ + \Sigma^-$  channel. The shaded areas display the uncertainties of the present calculations due to the uncertainties in the helicity photon couplings as in Fig. 3.

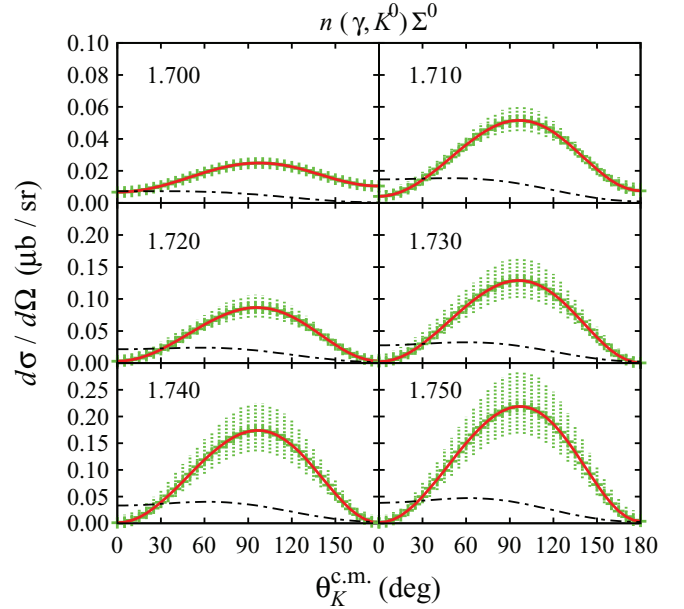


FIG. 8. (Color online) As in Fig. 7 but for the  $\gamma + n \rightarrow K^0 + \Sigma^0$  channel.

both predictions look very different in the whole energy range. In both cases, however, the present work indicates that smaller uncertainties can be obtained at energies very close to the threshold. Therefore, in both channels, measurement of the cross section close to the threshold is strongly recommended to further constrain the present model. The energy-dependent uncertainty exhibited by the total cross section given in Fig. 3 can be understood from the uncertainties shown in Figs. 7 and 8.

The  $\Sigma^0$  hyperon decays to a photon and a  $\Lambda$  hyperon. By analyzing the corresponding magnetic dipole ( $M1$ ) transition matrix element, which is proportional to  $\sigma \cdot \epsilon$ , where  $\sigma$  and  $\epsilon$  are the Pauli matrix and photon polarization vector, respectively, it can be shown that the polarization of  $\Lambda(P_\Lambda)$  is related to the polarization of  $\Sigma^0(P_\Sigma)$  through [62]

$$P_\Lambda = -\frac{1}{3}P_\Sigma. \quad (17)$$

Experimental data on  $K^+\Lambda$  and  $K^+\Sigma^0$  photoproduction seem to obey this relation.

As shown in the previous paper [9],  $P_\Lambda$  exhibits an inverted sine function, i.e., it has negative values near the forward angle, but changes sign near the backward angle. Therefore, in the case of  $\Sigma^0$  the expected polarization should display a sine function which is shown in Fig. 9, where it is obvious that the relation works nicely. The agreement of experimental data with the present work is probably not so surprising, because the data shown in Fig. 9 are included in the fitting data base. However, comparing this result with the prediction of Kaon-Maid demonstrates that the present work obeys the relation given by Eq. (17) and provides a substantial improvement in the case of the recoil polarization observable  $P$ .

As pointed out in Ref. [43], the relation between  $P_\Lambda$  and  $P_\Sigma$  given above seems to hold only at higher  $W$ . Indeed, it is found that, in a certain kinematics region, the relation fails to reproduce experimental data. In the present work, by

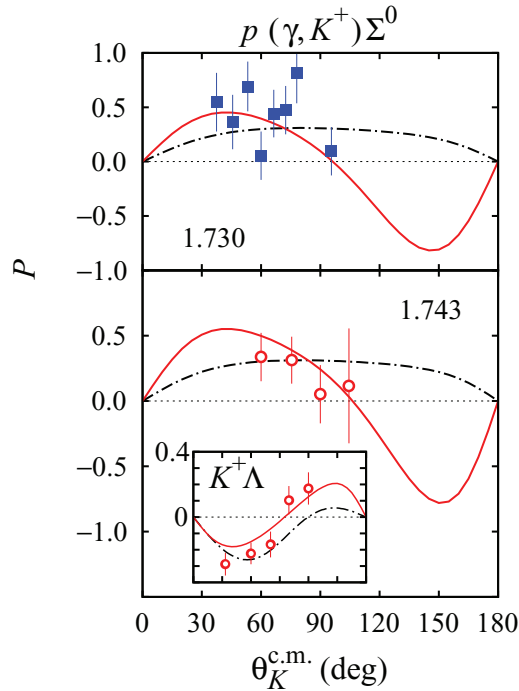


FIG. 9. (Color online) Recoil polarization in the  $\gamma + p \rightarrow K^+ + \Sigma^0$  process as a function of kaon scattering angle. Solid squares display the new CLAS data [43], whereas open circles exhibit the SAPHIR data [41]. Notation of the curves is as in Fig. 4. The inset shows a comparison between the previous calculation with Kaon-Maid and experimental data for the  $\gamma + p \rightarrow K^+ + \Lambda$  process [9].

comparing the solid curves in Fig. 9 and the result of my previous work (Fig. 6 of Ref. [9]), I find that this relation seems to work very well near the threshold region.

In spite of the nice agreement between experimental data and the present result, Fig. 9 also indicates that more data at backward and very forward angles are desired to support the present conclusion, especially that on the relation between the  $\Lambda$  and  $\Sigma^0$  polarizations near threshold.

The polarization of  $\Sigma^+$  in the  $\gamma + p \rightarrow K^0 + \Sigma^+$  process has been also measured with a similar technique, because  $\Sigma^+$  decays to  $p\pi^0$  and  $n\pi^+$  [51]. However, since the energy of measurement has been averaged between threshold and  $W = 1.95$  GeV, the corresponding energy is obviously beyond the present interest.

#### IV. NEW CRYSTAL BALL DATA

Recently, a new measurement of the  $K^+\Sigma^0$  differential cross section has been performed by the Crystal Ball Collaboration at MAMI with finer-energy bins [58]. For the present work, the result of this measurement increases the number of experimental data by 229 points. Since the number of data points in the database is almost doubled, the inclusion of these new data might have a significant influence on the previous result. To this end, I have refitted my previous model by including the new data. The relevant parameters obtained in this case, i.e., the photoproduction parameters,

TABLE V. Comparison between the extracted resonance photoproduction parameters obtained from fits to experimental data with and without the new Crystal Ball data [58] to those of the PDG estimate [1].

Resonance parameters	Without	With	PDG
<i>N</i> (1700) <i>D</i> <sub>13</sub>			
$M_R$ (MeV)	1716	1735	$1700 \pm 50$
$\Gamma_R$ (MeV)	250	100	$150^{+100}_{-50}$
$\beta_{K\Sigma}$	$3.0 \times 10^{-2}$	$3.0 \times 10^{-2}$	
$\phi$ (deg)	163	153	
$A_{1/2}(p)$ ( $10^{-3}$ GeV $^{-1/2}$ )	40	40	$15 \pm 25$
$A_{3/2}(p)$ ( $10^{-3}$ GeV $^{-1/2}$ )	-6	-18	$-15 \pm 25$
$\Delta$ (1700) <i>D</i> <sub>33</sub>			
$M_R$ (MeV)	1692	1693	$1700^{+50}_{-30}$
$\Gamma_R$ (MeV)	400	200	$300 \pm 100$
$\beta_{K\Sigma}$	$6.4 \times 10^{-5}$	$1.2 \times 10^{-4}$	
$\phi$ (deg)	63	90	
$A_{1/2}(p)$ ( $10^{-3}$ GeV $^{-1/2}$ )	170	149	$140 \pm 30$
$A_{3/2}(p)$ ( $10^{-3}$ GeV $^{-1/2}$ )	110	110	$140 \pm 30$
<i>N</i> (1710) <i>P</i> <sub>11</sub>			
$M_R$ (MeV)	1727	1740	$1710 \pm 30$
$\Gamma_R$ (MeV)	50	50	$100^{+150}_{-50}$
$\beta_{K\Sigma}$	$5.5 \times 10^{-3}$	$2.6 \times 10^{-3}$	
$\phi$ (deg)	40	42	
$A_{1/2}(p)$ ( $10^{-3}$ GeV $^{-1/2}$ )	43	57	$40 \pm 20$
<i>N</i> (1720) <i>P</i> <sub>13</sub>			
$M_R$ (MeV)	1700	1700	$1720^{+30}_{-20}$
$\Gamma_R$ (MeV)	150	150	$250^{+150}_{-100}$
$\beta_{K\Sigma}$	$1.2 \times 10^{-4}$	$4.2 \times 10^{-4}$	
$\phi$ (deg)	360	360	
$A_{1/2}(p)$ ( $10^{-3}$ GeV $^{-1/2}$ )	120	120	$100 \pm 20$
$A_{3/2}(p)$ ( $10^{-3}$ GeV $^{-1/2}$ )	120	120	$150 \pm 30$
$N$	331	560	
$\chi^2/N$	1.07	1.09	

are shown in Table V, where the result from the previous model (see Table IV) along with the corresponding PDG estimate are also displayed for comparison. Obviously, there are no dramatic changes in the parameters. Furthermore, in both fits (with and without the new Crystal Ball data) the fitted parameters are still consistent with the PDG values. Since the new measurement has been performed mostly in the backward direction, the corresponding effect is clearly more apparent in this kinematics, as shown in Fig. 10. Note that the new Crystal Ball data seem to be more consistent with the SAPHIR data [41] and, consequently, the result of including the new data at the corresponding kinematics is lowering the predicted differential cross section, approaching the prediction of Kaon-Maid [13].

#### V. RESULT FOR ELECTROPRODUCTION

Experimental data for low-energy kaon electroproduction were unavailable until the CLAS [50] and MAMI A1 collaborations [63] published their recent measurements. Note that,

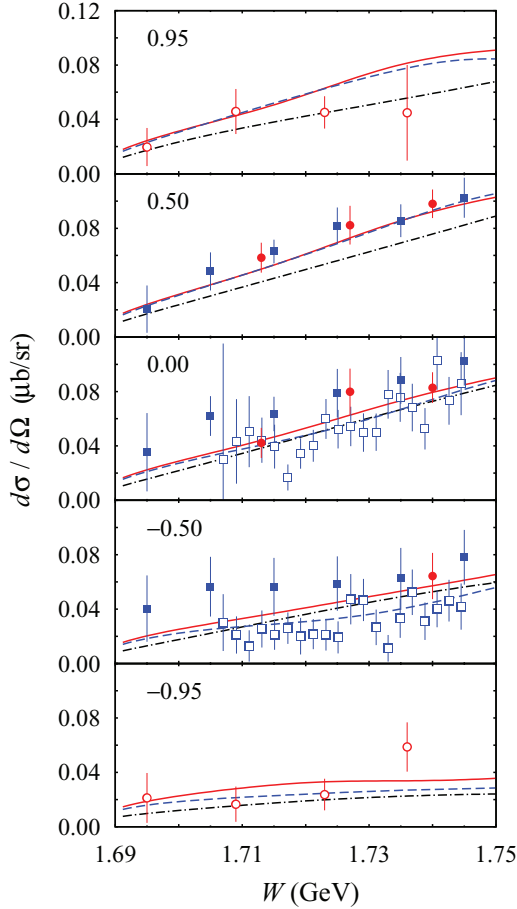


FIG. 10. (Color online) Differential cross section for the  $\gamma p \rightarrow K^+\Sigma^0$  channel. Solid and dashed curves are obtained from the calculations with excluding and including the new Crystal Ball data [58] in the database of the present analysis, respectively. Dash-dotted curves represent the predictions of Kaon-Maid [13]. Experimental data are from the SAPHIR (open circles [41]), CLAS (solid squares [43], solid circles [42]), and Crystal Ball (open squares [58]) collaborations. The corresponding value of  $\cos\theta$  is given in each panel.

in the old database, the lowest energy available is 1.930 GeV [64] and, therefore, they are irrelevant for the present study. Since the discussion on MAMI data is given in detail in the next section, I only focus on the CLAS data in this section.

In the present work, the  $Q^2$  dependence of the resonance multipoles reads [65]

$$A_{l\pm}(Q^2) = A_{l\pm}(0)(1 + \alpha_{N^*} Q^2)e^{-\beta_{N^*} Q^2}, \quad (18)$$

where  $\alpha_{N^*}$  and  $\beta_{N^*}$  are fit parameters given in Table IV. Note that this parametrization is used in Maid for the higher resonances [see Eq. (47) of Ref. [66]]. The values of  $\alpha_{N^*}$  and  $\beta_{N^*}$  given in Table IV are certainly not comparable to those of Maid, because in Maid the  $A_{1/2}$ ,  $A_{3/2}$ , and  $S_{1/2}$  amplitudes have different parametrization, whereas in the present work they are the same. Nevertheless, the same trend can be observed, e.g., in the case of  $N(1720)P_{13}$  the value of  $\alpha_{N^*}$  tends to be large, while the value of  $\beta_{N^*}$  is relatively small. In general, except for the  $N(1700)D_{13}$  resonance, it is found that the value of  $\alpha_{N^*}$  is

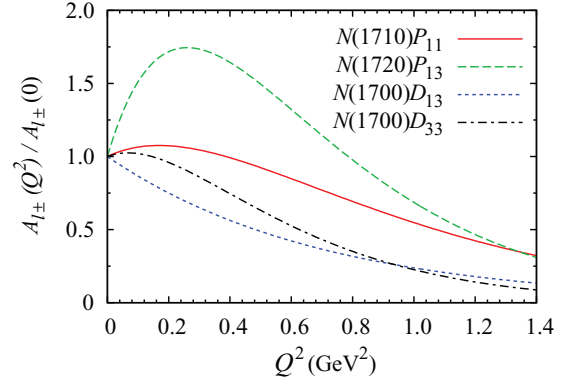


FIG. 11. (Color online)  $Q^2$  dependence of the resonance multipoles for the nucleon resonances used in the present analysis.

not zero. Therefore, as a consequence, as the  $Q^2$  increases the amplitudes  $A_{l\pm}(Q^2)$  increase from  $A_{l\pm}(0)$  at low  $Q^2$  and then monotonically decrease at higher  $Q^2$  values. This behavior, which is exhibited in Fig. 11 for the four nucleon resonances used in the present analysis, is important for the description of the longitudinal cross section given in Fig. 16 of Sec. VII, when I discuss the effect of  $K^0$  form factors.

Unlike the old data, the latest CLAS data have already been separated in terms of the unpolarized differential cross section  $\sigma_U \equiv d\sigma_T/d\Omega + \epsilon d\sigma_L/d\Omega$ , the transverse one  $\sigma_{TT} \equiv d\sigma_{TT}/d\Omega$ , and the longitudinal-transverse interference one  $\sigma_{LT} \equiv d\sigma_{LT}/d\Omega$ . Comparison of these data with the results of the present work and Kaon-Maid is shown in Fig. 12. In contrast to the prediction of Kaon-Maid, the CLAS data are remarkably much smaller, almost one order of magnitude. The over prediction of Kaon-Maid in the finite  $Q^2$  region will be discussed in the next section, when the result of the present work is compared with the new MAMI data. The agreement of the result of the present work with the CLAS data is clearly not surprising, because the data are fitted. However, I would like to note here that, in the case of unpolarized differential cross section (top panels), the cross section shows a certain structure in the angular distribution, i.e., a peak at  $\cos\theta \simeq 0.5$  and a tendency to increase at the backward direction. This indicates that the  $t$  and  $u$  channels should contain a significant longitudinal coupling in the case of electroproduction, which seems to disappear in the photoproduction case as displayed in Fig. 4. Figure 12 also shows that the virtual photoproduction cross section is in fact very small; much smaller than the predictions of isobar models as well as old data. Nevertheless, this is consistent with the photoproduction cross section, provided that there is no dramatic increase of the cross section in the  $Q^2$  distribution, which will be discussed in the next section.

Finally, it should also be noted that the longitudinal-transverse (LT) separation of the cross section has been also performed in Ref. [50]. The lowest energy available for this separation is 1.75 GeV, which is slightly beyond the upper limit of the present calculation. Nevertheless, for the sake of completeness and a future  $\sigma_L$ - $\sigma_T$  separation technique, the prediction of the present work along with the experimental data

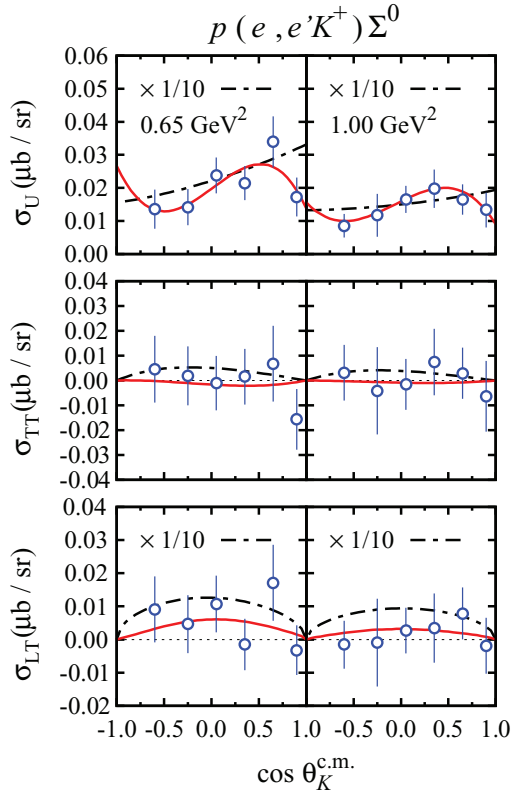


FIG. 12. (Color online) Separated differential cross sections for kaon electroproduction  $e + p \rightarrow e' + K^+ + \Sigma^0$  as a function of kaon scattering angles at  $W = 1.725 \text{ GeV}$  and for two different values of  $Q^2$  (the values are shown in the top panels). Experimental data are from the CLAS collaboration [50]. Notation of the curves is as in Fig. 4. Note that  $\sigma_i \equiv d\sigma_i/d\Omega$ , where  $i = U, TT$ , and  $LT$ . Predictions of Kaon-Maid in the top and bottom panels have been renormalized by a factor of  $\frac{1}{10}$  in order to fit on the scale.

is exhibited in Fig. 13, where the prediction of Kaon-Maid is also shown for comparison. In general, the prediction of the present work provides a fair agreement with experimental data. Interestingly, Kaon-Maid predicts a large and forward peaking longitudinal cross section, whereas in the case of transverse cross section it shows very different behavior. It can obviously be seen that the shape of unpolarized cross section of both models shown in the upper panel of Fig. 12 clearly originates from the separated ones, as reflected by Fig. 13. It is also apparent that the result of the present calculation overestimates the data near forward angles. This happens presumably because the corresponding energy is already beyond the upper limit of current study. However, at this kinematics the longitudinal cross section data have negative values, which is certainly difficult to be reproduced by the model, since by definition  $\sigma_L \propto |H_5|^2 + |H_6|^2 \geq 0$ , where  $H_5$  and  $H_6$  are functions of the longitudinal CGLN amplitudes  $F_5$  and  $F_6$  [68]. Therefore, the present calculation recommends a new analysis on the  $\sigma_L$ - $\sigma_T$  separation by imposing a new constraint on the longitudinal cross section, i.e.,  $\sigma_L \geq 0$ . Such a constraint could be expected to reduce some uncertainties in the separation technique given in Ref. [50].

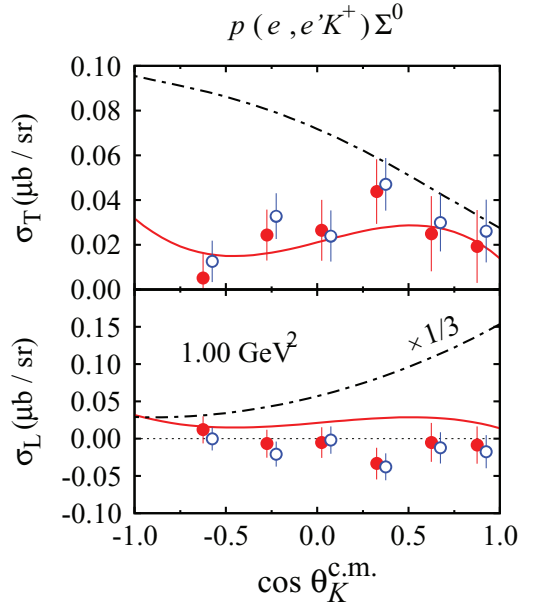


FIG. 13. (Color online) As in Fig. 12, but for separated transverse (T) and longitudinal (L) differential cross sections at  $W = 1.75 \text{ GeV}$  and  $Q^2 = 1.0 \text{ GeV}^2$ . Note that all experimental data shown in this Figure [50] are not used in the fit. Solid and open circles indicate two different methods of the  $\sigma_L$ - $\sigma_T$  separation, which are slightly shifted for the sake of visibility. Further explanation of the data can be found in Ref. [50] as well as in the JLab Experiment CLAS Database [67]. In the lower panel, the prediction of Kaon-Maid has been renormalized by a factor of  $\frac{1}{3}$  to fit on the scale.

## VI. NEW MAMI DATA AT LOW $Q^2$

Recently, the A1 Collaboration at MAMI, Mainz, has measured the kaon electroproduction process  $e + p \rightarrow e' + K^+ + \Sigma^0$  close to the production threshold and at very low virtual photon momentum transfers, i.e.,  $Q^2 = 0.030$  to  $0.055 \text{ GeV}^2$  [63]. These new data are obviously of interest because they can be expected to provide new information on the transition between photo- and electroproduction process. This transition corresponds to the longitudinal coupling in the process and therefore is very crucial for investigation of the electromagnetic form factors, especially those of kaons and hyperons for which no stable target exists.

More than a decade ago, Niculescu *et al.* [69] measured the  $e + p \rightarrow e' + K^+ + \Lambda$  process and found that the longitudinal cross section  $d\sigma_L/d\Omega$  at  $Q^2 = 0.52 \text{ GeV}^2$  is significantly large, almost as large as the transverse one  $d\sigma_T/d\Omega$ . To reproduce these data an isobar model must dramatically increase both cross sections from the photon point up to a certain value of  $Q^2$  (see Fig. 5 of Ref. [70]). The revised analysis [71] of the same data found that the longitudinal cross section is much smaller than the previous ones. A recent result from JLab improves these data significantly [50]. However, in spite of this substantial improvement, extrapolation of the combined cross section  $d\sigma_T/d\Omega + \epsilon d\sigma_L/d\Omega$  to the photon point overshoots the experimental photoproduction data [50]. Furthermore, due to the detector properties, there were no data points available in the range of  $Q^2 = 0.0$  to  $0.5 \text{ GeV}^2$ . Thus,

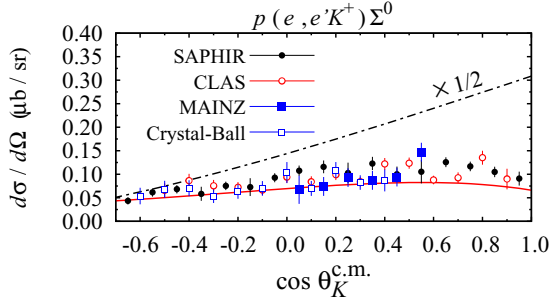


FIG. 14. (Color online) Comparison between new electroproduction data at  $W = 1.75$  GeV and  $Q^2 = 0.036$  GeV<sup>2</sup> from MAMI [63] with photoproduction data from the SAPHIR [41], CLAS [42], and Crystal Ball [58] collaborations, along with the prediction of the present work (solid line) and Kaon-Maid (dash-dotted line). The prediction of Kaon-Maid has been renormalized by a factor of  $\frac{1}{2}$  to fit on the scale. Note that all data shown in this figure are not used in the fitting process since the corresponding energies are higher than the upper energy limit. Furthermore, the predicted differential cross sections are calculated for the electroproduction case ( $Q^2 = 0.036$  GeV<sup>2</sup>).

the problem of dramatic increase in the cross sections remained unsolved.

Although fit to the different electroproduction data [64], the  $Q^2$  evolution of the cross section for the  $e + p \rightarrow e' + K^+ + \Sigma^0$  channel of Kaon-Maid exhibits the same behavior. However, this situation seems to be improved after the A1 Collaboration published its result [63]. As shown in Figs. 14 and 15, the transition between photo- and electroproduction is found to be very smooth. In fact, within their error bars the data seem to be consistent. Nevertheless, unlike the prediction of Kaon-Maid, the present calculation predicts an excellent agreement with the new MAMI data, as shown clearly in Fig. 14.

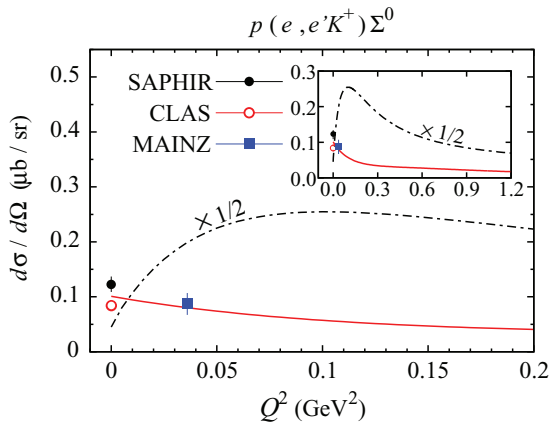


FIG. 15. (Color online) As in Fig. 14 but for the virtual photon momentum transfer squared  $Q^2$  distribution calculated with  $W = 1.75$  GeV,  $\cos \theta = 0.35$ ,  $\epsilon = 0.4$ , and  $\Phi = 0^\circ$ . See Sec. VI of Ref. [9] for a detailed explanation of the electroproduction parameters. The inset shows a comparison between Kaon-Maid and the result of the present work for higher  $Q^2$  values.

Figure 15 shows that the differential cross section just monotonically falls off as the virtual photon momentum  $Q^2$  increases from zero, in contrast to the prediction of Kaon-Maid. The latter is understandable, since it was fit to the old data, which are scarce, have large error bars, and are scattered over a wide range of kinematics [64]. Thus, Fig. 15 indicates that, for the low-energy case, the longitudinal coupling in the  $K^+\Sigma^0$  channel is relatively small and the shape of the electroproduction cross section is practically driven by the conventional electromagnetic form factors. Obviously, more electroproduction data with the same kinematics but within the range of  $Q^2 = 0.05$  to  $0.5$  GeV<sup>2</sup> are needed to support the present conclusion. Such experimental data will be available in the near future from the MAMI Collaboration [72].

## VII. ELECTROMAGNETIC FORM FACTOR OF NEUTRAL KAON

In the previous paper [10] I investigated the effect of the  $K^0$  charge (electromagnetic) form factor on the longitudinal differential cross section of the  $e + n \rightarrow e' + K^0 + \Lambda$  process. By using the light-cone quark (LCQ) model [73] it was found that the form factor can raise the longitudinal cross section by up to 50%. In view of this promising result, it could be expected that experimental data with about 10% error bars would be able to experimentally prove the existence of this form factor in the process and, simultaneously, to select the appropriate  $K^0$  form factor.

Given the large effect of  $K^0$  charge form factor on the  $K^0\Lambda$  electroproduction longitudinal cross section, it is clearly of interest to investigate the effect on both  $K^0\Sigma^+$  and  $K^0\Sigma^0$  electroproduction channels studied in the present work, where the neutral kaon can directly interact with the virtual photon in the  $t$  channel. For this purpose I use the same form factor models as in my previous study [10], i.e., the LCQ model [73] and the quark-meson vertex (QMV) model [74,75].

The result for both  $K^0\Sigma^+$  and  $K^0\Sigma^0$  isospin channels is shown in Fig. 16. Obviously, the effect found in both cases is milder than that found in the  $K^0\Lambda$  channel [10], which is understandable, since the form factor in the present case is multiplied by the  $g_{K\Sigma N}$  coupling constant. As shown in Table III, the value of  $g_{K\Sigma N}$  in the present case is about 60% smaller than that of  $g_{K\Lambda N}$ . Furthermore, I also note that, in the case of the  $K^0\Lambda$  channel, contribution from the background terms is significantly larger than that of the resonance terms (see Fig. 1 of Ref. [10]). This is not the case in both the  $K^0\Sigma^+$  and  $K^0\Sigma^0$  channels (see Fig. 2). Nevertheless, it is worth mentioning that, in both channels, there is moderate sensitivity to these form factors in the range of  $Q^2 \approx 0.4$  to  $1.0$  GeV<sup>2</sup>, where the largest one (up to about 10%) originates from the LCQ model. The latter corroborates the finding of my previous work [10].

From the above result I could conclude that, in the kaon electroproduction process, only the  $e + n \rightarrow e' + K^0 + \Lambda$  channel seems to be the most promising process for investigating the neutral kaon charge form factor. However, due to the lack of free neutron target, the  $e + p \rightarrow e' + K^0 + \Sigma^+$  channel shown in the upper panel of Fig. 16 could become another alternative for this purpose, provided that more

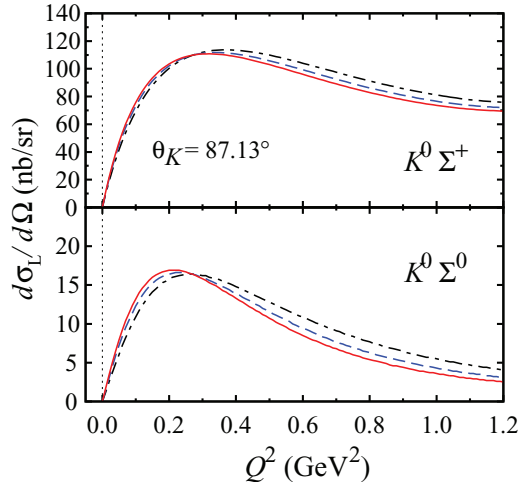


FIG. 16. (Color online) Longitudinal differential cross section of (a) the neutral kaon electroproduction  $e + p \rightarrow e' + K^0 + \Sigma^+$  and (b)  $e + n \rightarrow e' + K^0 + \Sigma^0$ , as a function of the virtual photon momentum squared  $Q^2$  at  $W = 1.72$  GeV and for the kaon scattering angle  $87.13^\circ$ . Solid lines show the calculation with a  $K^0$  form factor obtained in the LCQ model [73] while dashed lines are obtained by using the QMV model [74,75]. The dash-dotted lines are obtained from a computation with the  $K^0$  pole excluded.

precise experimental measurements with about 5% error bars along with a more accurate  $\sigma_L$ - $\sigma_T$  separation technique were available. Such a measurement is presumably suitable for a future experiment at MAMI in Mainz.

### VIII. SUMMARY AND CONCLUSIONS

I analyzed the elementary photo- and electroproduction of  $K\Sigma$  for all four possible isospin channels near their production thresholds. To this end I have used an isobar model based on suitable Feynman diagrams for the background terms, for which all unknown parameters such as hadronic coupling constants and electromagnetic form factor cutoffs were extracted from experimental data. For the resonance terms I used the Breit-Wigner form of multipoles, in which the values of photon couplings were taken from the PDG. It is found that, near the thresholds, the four isospin channels of

$K\Sigma$  photoproduction are mostly driven by their background terms, instead of the resonance terms as in the case of  $K\Lambda$  photoproduction. Furthermore, in contrast to the  $K^+\Lambda$  channel, the present study indicates that the hyperon resonances do not play an important role in  $K\Sigma$  channels.

Whereas the result of the present calculation for the proton channels provides a nice agreement with experimental data as well as a substantial improvement of my previous work, the prediction of the present analysis for the neutron channels are plagued with some uncertainties that originate from the uncertainties in the values of the helicity photon couplings given by PDG. The present study also proves the validity of the relation between  $\Lambda$  and  $\Sigma^0$  polarizations, i.e.,  $P_\Lambda = -(\frac{1}{3})P_\Sigma$ , at energies near thresholds.

The extracted longitudinal differential cross section from the CLAS experiment is found to be too small. This finding suggests the necessity for a new extraction method that imposes the condition that the cross section values are always positive. The new MAMI electroproduction data at very low  $Q^2$  can be nicely reproduced, although they were not included in the present analysis. These new data support the smooth transition behavior from photo- to electroproduction, which is exhibited by the present work, but not by Kaon-Maid. Therefore, the large longitudinal term coming from the  $D_{13}(1895)$  resonance in Kaon-Maid is not proven.

Finally, the effect of the neutral kaon charge form factor on the longitudinal cross sections of the  $K^0\Sigma^+$  and  $K^0\Sigma^0$  electroproduction channels is found to be smaller than that obtained in the  $K^0\Lambda$  channel. Nevertheless, the  $K^0\Sigma^+$  electroproduction channel could become an alternative process for investigation of this form factor, provided that the corresponding longitudinal cross section can be accurately extracted.

### ACKNOWLEDGMENTS

The author thanks T. Jude and D. Watts for providing him with the new Crystal Ball  $K\Sigma$  data. Useful discussion with I. I. Strakovsky and R. Schumacher is gratefully acknowledged. This work was partly supported by the Research-Cluster-Grant-Program of the University of Indonesia, under Contract No. 1709/H2.R12/HKP.05.00/2014.

- 
- [1] K. A. Olive *et al.* (Particle Data Group Collaboration), *Chin. Phys. C* **38**, 090001 (2014).
  - [2] H. Haberzettl, C. Bennhold, T. Mart, and T. Feuster, *Phys. Rev. C* **58**, R40(R) (1998).
  - [3] R. M. Davidson and R. Workman, *Phys. Rev. C* **63**, 025210 (2001).
  - [4] T. Mart and A. K. Sari, *Mod. Phys. Lett. A* **28**, 1350054 (2013).
  - [5] M. Guidal, J. M. Laget, and M. Vanderhaeghen, *Nucl. Phys. A* **627**, 645 (1997).
  - [6] T. Mart and T. Wijaya, *Acta Phys. Pol. B* **34**, 2651 (2003).
  - [7] T. Corthals, T. Van Cauteren, J. Ryckebusch, and D. G. Ireland, *Phys. Rev. C* **75**, 045204 (2007).
  - [8] L. De Cruz, J. Ryckebusch, T. Vranx, and P. Vancraeyveld, *Phys. Rev. C* **86**, 015212 (2012).
  - [9] T. Mart, *Phys. Rev. C* **82**, 025209 (2010).
  - [10] T. Mart, *Phys. Rev. C* **83**, 048203 (2011).
  - [11] S. Steininger and U. G. Meissner, *Phys. Lett. B* **391**, 446 (1997).
  - [12] M. K. Cheoun, B. S. Han, B. G. Yu, and I. T. Cheon, *Phys. Rev. C* **54**, 1811 (1996).
  - [13] Available at the Maid homepage <http://www.kph.uni-mainz.de/MAID/kaon/kaonmaid.html>. The published versions can be found in Refs. [27, 70] and in T. Mart, *Phys. Rev. C* **62**, 038201 (2000).
  - [14] R. A. Arndt, Ya. I. Azimov, M. V. Polyakov, I. I. Strakovsky, and R. L. Workman, *Phys. Rev. C* **69**, 035208 (2004).

- [15] R. A. Arndt, W. J. Briscoe, M. W. Paris, I. I. Strakovsky, and R. L. Workman, *Chin. Phys. C* **33**, 1063 (2009).
- [16] T. Mart, *Phys. Rev. D* **83**, 094015 (2011); **88**, 057501 (2013).
- [17] D. Diakonov, V. Petrov, and M. Polyakov, *Z. Phys. A: Hadrons Nucl.* **359**, 305 (1997).
- [18] A. Kiswandhi and S. N. Yang, *Phys. Rev. C* **86**, 015203 (2012); **86**, 019904(E) (2012).
- [19] B. Saghai, J.-C. David, B. Julia-Diaz, and T.-S. H. Lee, *Eur. Phys. J. A* **31**, 512 (2007).
- [20] S. Janssen, J. Ryckebusch, D. Debruyne, and T. Van Cauteren, *Phys. Rev. C* **65**, 015201 (2001).
- [21] D. G. Ireland, S. Janssen, and J. Ryckebusch, *Nucl. Phys. A* **740**, 147 (2004).
- [22] B. Borasoy, P. C. Bruns, U.-G. Meissner, and R. Nissler, *Eur. Phys. J. A* **34**, 161 (2007).
- [23] E. Klempt and J.-M. Richard, *Rev. Mod. Phys.* **82**, 1095 (2010).
- [24] V. A. Nikonov, A. V. Anisovich, E. Klempt, A. V. Sarantsev, and U. Thoma, *Phys. Lett. B* **662**, 245 (2008).
- [25] A. V. Anisovich, E. Klempt, V. A. Nikonov, A. V. Sarantsev, and U. Thoma, *Eur. Phys. J. A* **47**, 27 (2011).
- [26] A. V. Anisovich, R. Beck, E. Klempt, V. A. Nikonov, A. V. Sarantsev, and U. Thoma, *Eur. Phys. J. A* **48**, 15 (2012).
- [27] T. Mart and C. Bennhold, *Phys. Rev. C* **61**, 012201 (1999).
- [28] O. V. Maxwell, *Phys. Rev. C* **85**, 034611 (2012); **86**, 064612 (2012).
- [29] L. De Cruz, T. Vranx, P. Vancraeyveld, and J. Ryckebusch, *Phys. Rev. Lett.* **108**, 182002 (2012).
- [30] S. Capstick and W. Roberts, *Phys. Rev. D* **49**, 4570 (1994).
- [31] SAPHIR Collaboration, M. Q. Tran *et al.*, *Phys. Lett. B* **445**, 20 (1998).
- [32] T. Mart and M. J. Kholili, *Phys. Rev. C* **86**, 022201(R) (2012).
- [33] M. Kawaguchi and M. J. Moravcsik, *Phys. Rev.* **107**, 563 (1957).
- [34] A. Fujii and R. E. Marshak, *Phys. Rev.* **107**, 570 (1957).
- [35] T. Mart, C. Bennhold, and C. E. Hyde-Wright, *Phys. Rev. C* **51**, R1074(R) (1995).
- [36] P. Bydžovský and T. Mart, *Phys. Rev. C* **76**, 065202 (2007).
- [37] S. Janssen, J. Ryckebusch, D. Debruyne, and T. Van Cauteren, *Phys. Rev. C* **66**, 035202 (2002).
- [38] Zhenping Li, MaWei-Hsing, and Lin Zhang, *Phys. Rev. C* **54**, R2171(R) (1996).
- [39] T. Mart and A. Sulaksono, *Phys. Rev. C* **74**, 055203 (2006).
- [40] T. Mart, *Int. J. Mod. Phys. E* **19**, 2343 (2010).
- [41] K.-H. Glander *et al.*, *Eur. Phys. J. A* **19**, 251 (2004).
- [42] R. Bradford *et al.* (CLAS Collaboration), *Phys. Rev. C* **73**, 035202 (2006).
- [43] B. Dey *et al.* (CLAS Collaboration), *Phys. Rev. C* **82**, 025202 (2010).
- [44] K. Nakamura (Particle Data Group), *J. Phys. G: Nucl. Part. Phys.* **37**, 075021 (2010).
- [45] T. Mart, *Few-Body Syst.* **54**, 1167 (2013).
- [46] T. Mart, *Genshikaku Kenkyu* **57**, Suppl. 3, 93 (2013).
- [47] D. Drechsel, O. Hanstein, S. S. Kamalov, and L. Tiator, *Nucl. Phys. A* **645**, 145 (1999).
- [48] T. Mart, *Phys. Rev. C* **87**, 042201(R) (2013).
- [49] J. W. C. McNabb *et al.* (CLAS Collaboration), *Phys. Rev. C* **69**, 042201 (2004); J. W. C. McNabb, Ph.D. Thesis, Carnegie Mellon University, 2002 (unpublished).
- [50] P. Ambrozewicz *et al.*, *Phys. Rev. C* **75**, 045203 (2007).
- [51] R. Lawall *et al.*, *Eur. Phys. J. A* **24**, 275 (2005).
- [52] M. Sumihama *et al.*, *Phys. Rev. C* **73**, 035214 (2006).
- [53] H. Kohri *et al.*, *Phys. Rev. Lett.* **97**, 082003 (2006).
- [54] T. Mart and N. Nurhadiansyah, *Few-Body Syst.* **54**, 1729 (2013).
- [55] R. A. Adelseck and B. Saghai, *Phys. Rev. C* **42**, 108 (1990).
- [56] K. Tsukada *et al.*, *Phys. Rev. C* **78**, 014001 (2008); **83**, 039904 (2011).
- [57] S. Anefalos Pereira *et al.* (CLAS Collaboration), *Phys. Lett. B* **688**, 289 (2010).
- [58] T. C. Jude *et al.*, *Phys. Lett. B* **735**, 112 (2014).
- [59] H. Thom, *Phys. Rev.* **151**, 1322 (1966).
- [60] P. Singer and G. A. Miller, *Phys. Rev. D* **33**, 141 (1986).
- [61] R. A. Schumacher (private communication).
- [62] R. A. Schumacher, *Hadron and Strangeness Nuclear Physics with Electron and Photon Beams, lecture given at the International School for Strangeness Nuclear Physics, February 12–18, 2012, J-PARC, Tokai & Tohoku University, Sendai, Japan*, see <http://lambda.phys.tohoku.ac.jp/snpssc2012/index2.html>; R. Gatto, *Phys. Rev.* **109**, 610 (1958).
- [63] P. Achenbach *et al.*, *Eur. Phys. J. A* **48**, 14 (2012).
- [64] C. N. Brown *et al.*, *Phys. Rev. Lett.* **28**, 1086 (1972); T. Azemoon *et al.*, *Nucl. Phys. B* **95**, 77 (1975); C. J. Bebek *et al.*, *Phys. Rev. D* **15**, 594 (1977); P. Brauel *et al.*, *Z. Phys. C: Part. Fields* **3**, 101 (1979).
- [65] T. Mart and A. Sulaksono, [arXiv:nucl-th/0701007](https://arxiv.org/abs/nucl-th/0701007).
- [66] D. Drechsel, S. S. Kamalov, and L. Tiator, *Eur. Phys. J. A* **34**, 69 (2007).
- [67] <http://clasweb.jlab.org/physicsdb/>.
- [68] G. Knöchlein, D. Drechsel, and L. Tiator, *Z. Phys. A: Hadrons Nucl.* **352**, 327 (1995).
- [69] G. Niculescu *et al.*, *Phys. Rev. Lett.* **81**, 1805 (1998).
- [70] C. Bennhold, H. Haberzettl, and T. Mart, [arXiv:nucl-th/9909022](https://arxiv.org/abs/nucl-th/9909022).
- [71] R. M. Moring *et al.*, *Phys. Rev. C* **67**, 055205 (2003).
- [72] P. Achenbach (private communication).
- [73] C. Bennhold, H. Ito, and T. Mart, in *Proceedings of the 7th International Conference on the Structure of Baryons* (Santa Fe, New Mexico, 1995), p. 323.
- [74] W. W. Buck, R. Williams, and H. Ito, *Phys. Lett. B* **351**, 24 (1995).
- [75] H. Ito and F. Gross, *Phys. Rev. Lett.* **71**, 2555 (1993).